Journal of Biomechanics 49 (2016) 1290–1304

Contents lists available at ScienceDirect

Journal of Biomechanics

journal homepage: www.elsevier.com/locate/jbiomech
www.JBiomech.com

A computational framework for particle and whole cell tracking applied to a real biological dataset

Feng Wei Yang [a,*], Chandrasekhar Venkataraman [b], Vanessa Styles [a], Verena Kuttenberger [c], Elias Horn [c], Zeno von Guttenberg [c], Anotida Madzvamuse [a]

[a] Department of Mathematics, University of Sussex, UK
[b] School of Mathematics & Statistics, University of St Andrews, UK
[c] ibidi GmbH Am Klopferspitz 19, 82152 Martinsried, Germany

ARTICLE INFO

Article history:
Accepted 3 February 2016

Keywords:
Cell tracking
Segmentation
Particle tracking
Optimal control
Phase-contrast microscopy
Geometric evolution law

ABSTRACT

Cell tracking is becoming increasingly important in cell biology as it provides a valuable tool for analysing experimental data and hence furthering our understanding of dynamic cellular phenomena. The advent of high-throughput, high-resolution microscopy and imaging techniques means that a wealth of large data is routinely generated in many laboratories. Due to the sheer magnitude of the data involved manual tracking is often cumbersome and the development of computer algorithms for automated cell tracking is thus highly desirable.

In this work, we describe two approaches for automated cell tracking. Firstly, we consider particle tracking. We propose a few segmentation techniques for the detection of cells migrating in a non-uniform background, centroids of the segmented cells are then calculated and linked from frame to frame via a nearest-neighbour approach. Secondly, we consider the problem of whole cell tracking in which one wishes to reconstruct in time whole cell morphologies. Our approach is based on fitting a mathematical model to the experimental imaging data with the goal being that the physics encoded in the model is reflected in the reconstructed data. The resulting mathematical problem involves the optimal control of a phase-field formulation of a geometric evolution law. Efficient approximation of this challenging optimal control problem is achieved via advanced numerical methods for the solution of semilinear parabolic partial differential equations (PDEs) coupled with parallelisation and adaptive resolution techniques.

Along with a detailed description of our algorithms, a number of simulation results are reported on. We focus on illustrating the effectivity of our approaches by applying the algorithms to the tracking of migrating cells in a dataset which reflects many of the challenges typically encountered in microscopy data.

1. Introduction

Cell migration is an essential part of many normal biological processes and diseases (Friedl and Gilmour, 2009). The dynamics of collective-cell movement, cell-to-cell interactions as well as interactions between cells and the extracellular environment are closely related to the bio-chemical and bio-mechanical properties of a single cell (Friedl and Alexander, 2011; Weigelin et al., 2012; Wolf et al., 2013).

Bio-laboratories nowadays produce a huge amount of data in multi-dimensions (both in space and time) e.g., microscopy images, that is far beyond the capacity of manual analysis in order to make informed decisions about cell shape evolution and migration trajectories (Maska et al., 2014). Hence, one demands computationally fully-automated cell tracking procedures. The focus of this work is to present techniques to solve the challenging problems that arise when one seeks to automate reconstruction of cell shape evolution and cell migration trajectories from static data.

We present two different approaches; the first approach involves an algorithm for single particle tracking that is successively applied for multiple particles in which the most challenging step is detecting cells migrating over a substrate where the intensities of both cells and background, using the microscopy and imaging techniques under consideration, are (spatially) non-uniform and the second approach seeks to address the problem of whole cell tracking in

* Corresponding author.
E-mail addresses: F.W.Yang@sussex.ac.uk (F.W. Yang), cv28@st-andrews.ac.uk (C. Venkataraman), V.Styles@sussex.ac.uk (V. Styles), vkuttenberger@ibidi.de (V. Kuttenberger), ehorn@ibidi.de (E. Horn), zguttenberg@ibidi.de (Z. von Guttenberg), A.Madzvamuse@sussex.ac.uk (A. Madzvamuse).

http://dx.doi.org/10.1016/j.jbiomech.2016.02.008

which cell shape evolution is reconstructed from static imaging data, with the corresponding recovered data generated by fitting a mathematical model, derived from physical principles, to the data (Croft et al., 2014; Blazakis et al., 2015; Yang et al., 2015). For particle tracking, described in Section 3, we treat each cell as a single object (i.e., a dot) and seek to determine the speed and direction of cell centroid trajectories. The latter approach, illustrated in Section 4, focusses on recovering dynamic cell morphologies and typically is of use to study a single cell or multiple cells in a low density setting. This resulting mathematical problem is formulated as the optimal control of a geometric evolution law (DuChateau and Zachmann, 1989; Rektorys, 1999).

2. Cell culture and microscopy

As mentioned above, to test the performance of our algorithms, we apply them to an experimental dataset generated in the labs of ibidi GmbH (2015). We summarise the details of the experimental protocol used to generate the biological data used in this study.

The human fibrosarcoma cell line HT-1080 (obtained from DSMZ, Germany) was grown in Dulbecco's modified Eagle's Medium (DMEM, Sigma-Aldrich) supplemented with 10% fetal bovine serum (FBS, Sigma-Aldrich) at 37 °C and 5% CO_2. Cells were grown to 80% confluence, trypsinised, and filled into the chemotaxis chambers of the μ-Slide Chemotaxis ibiTreat (ibidi GmbH, Germany) at a density of 3×106 cells/ml. To perform a migration experiment without chemoattractant both reservoirs and the channel were filled with DMEM with 5% FBS. Video microscopy was performed using a Nikon TiE microscope equipped with a 4x phase-contrast objective and the pixel size 1.66 µm/px. The time-lapse interval was ten minutes over a time period of 24 h.

3. Segmentation and particle tracking

In this setting, the first step is to individually represent each cell by a single dot (typically the centre of the segmented cell), this is achieved in a two-part process, first the cells are segmented from background and noise effects, then each individual cell is detected and labelled. The second step is to determine the correspondence between cells from one frame to the other, this is typically done by linking the corresponding dots between imaging frames. After a brief review of some existing algorithms for segmentation, we describe our algorithms for each step and illustrate their effectiveness on the experimental dataset under consideration in this work.

3.1. A review of segmentation techniques

In phase-contrast microscopy, phase shifts of the specimen are transformed into amplitude (intensity) shifts, thus permitting objects that are usually almost invisible (e.g. cells), to be optically visible. Furthermore, this also results in possible background inhomogeneities and various noise effects also becoming more prominent. Certain techniques are necessary to help identify cells and image segmentation, so that a common approach can be employed. Image segmentation is defined as a process of partitioning an image into homogeneous groups such that each region is homogeneous but that no union of two adjacent regions is homogeneous (Pal and Pal, 1993). In this section, we describe some widely used segmentation techniques from the literature.

For completeness, there is an alternative, namely fluorescent microscopy, that has been commonly used to study processes in the physiological context of intact living cells (Pepperkok and Ellenberg, 2006). The basic idea is to bind some fluorescent stains with the DNA of the targeted cellular components, for example, the nucleus of the cell. Since the light from the fluorescent stains have specific wavelength (Grynkiewicz et al., 1985), with correct imaging techniques, it is possible to only capture these illuminated components, in turn helping identify the positions of cells. In principle, it is possible to label cells in fluorescent microscopy with no or little image segmentation. On the other hand, comparing to phase-contrast microscopy, disadvantages of fluorescent microscopy include that the extra staining requires further manual input thereby prolonging the whole process and that, the fluorescence can only illuminate for a certain length of time, namely its bleach rate (Denk et al., 1990), thus is unfavourable for longer experiments. Moreover, advanced segmentation techniques are still required if the illuminated components collide or overlap.

We illustrate a typical phase-contrast image from the biological dataset used in this work in Fig. 1 and the full length video (*raw_data.avi*) is included in the supplementary material.

Depending on the objective lens, the phase-contrast technique works in a certain range of phase shifts only. If the shift is too big, artefacts are created. The halo effect is a common phase shift artefact. For example, when a cell rounds up (such as when undergoing cell division), a bright halo is often visible around the cell. If cells or cellular structures like filopodia are less thick and flat on the substrate they are optically dark.

In Fig. 1, we identify (by arrows in the figure) three main sets of distinct features representing the cells:

(a) cells can be clearly observed, they have little or no halo artefacts and the centre generally is the brightest with the highest intensity value;

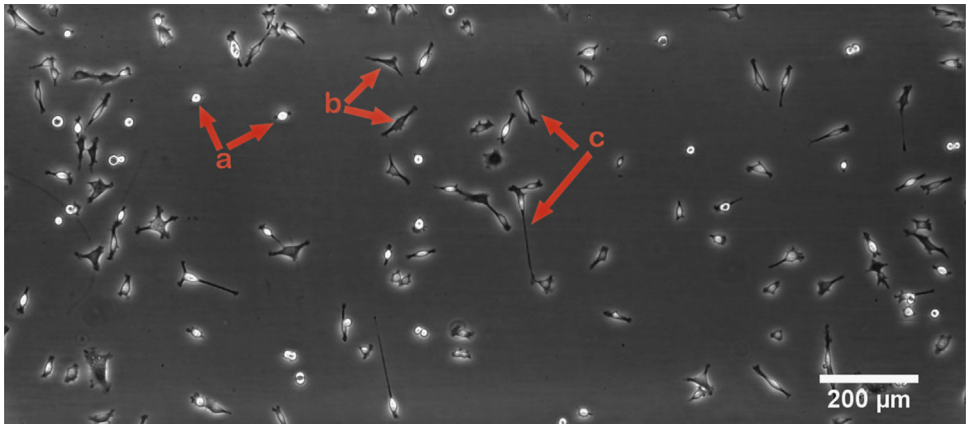

Fig. 1. A typical phase-contrast image from the biological dataset. Arrows and three letters are used to identify cells with distinct features.

(b) the cells are (partially and relatively) flat, thus they appear darker (especially in the centre) but have a bright halo artefact.
(c) various intensities appear brighter in the (thicker) centre of the cell and darker in (flatter) structures like filopodia.

In the images, the cells show a lot of filopodia. This is normal for this cell type. Filopodia arise naturally in many migrating cell types and hence it is important that cell tracking algorithms are capable of dealing with such features.

In addition to these different cell features, we also have a background with varying intensities. Although these features may be easily determined and categorised by a human, due to their digital representations and a computer's limited ability for pattern recognition, they are very difficult for a computer to recognise.

This problem can be thought of in the context of the recent IEEE International Symposium on Biomedical Imaging 2013 Cell Tracking Challenge, where six real-cell datasets were presented, each with its own difficulties and challenges in terms of segmentation (Maska et al., 2014). Our current images have most of the hallmarks of these difficulties and hence give rise to challenges for any algorithms. The main challenges are “cell blebbing features” (i.e. the expansion of a bulge of membrane), “cells entering and leaving the field of view”, “large time steps” (i.e., large displacements and morphological changes between frames), “colliding of elongated cells”, “frequent cell collisions”, “various intensity”, “prominent nucleoli” and “mitoses” (Maska et al., 2014).

One of the six datasets in the Cell Tracking Challenge was C3DL-MDA231 (Maska et al., 2014; Cell Tracking Challenge Datasets, 2015) which uses human breast carcinoma cells infected with a pMSCV vector including the GFP sequence, embedded in a collagen matrix. The cells in this dataset are elongated, fast moving and colliding and as such present similar challenges to the ones we are facing in the current dataset. However the dataset in C3DL-MDA231 does not have the halo artefacts or heterogeneous background that our datasets have. Since the most competitive method from the challenge series, KTH-SE (Maska et al., 2014), used global thresholding followed by a watershed transform for splitting clusters as their segmentation technique, based on the results presented in Figs. 2 and 3 we believe that this technique may not work well on our problem, because of the heterogeneous background and the halo artefacts.

In Hand et al. (2009), a number of open source software packages for cell segmentation and tracking are discussed. We use two of these packages to demonstrate that global thresholding is suboptimal for the dataset we are currently working on. In Fig. 2, we provide the segmented image from the data shown in Fig. 1 using ImageJ's default option of segmentation (Schneider et al., 2012). It can be seen from this figure, that the middle part of the background is darker, and the background at the top-left corner is much lighter. If we choose parameters that are good for the top-left corner, for example, cells at the middle may disappear. This problem occurs throughout the large selection of the global thresholding techniques provided by ImageJ. An example using the so-called “Otsu” technique (Otsu, 1979) is demonstrated in Fig. 3. The reason for this poor performance is because the assumptions made within these techniques do not include varying background intensities.

Cell segmentation is a large scientific research field where an enormous number of algorithms exist. Throughout our literature review process, it appears to us that each segmentation technique

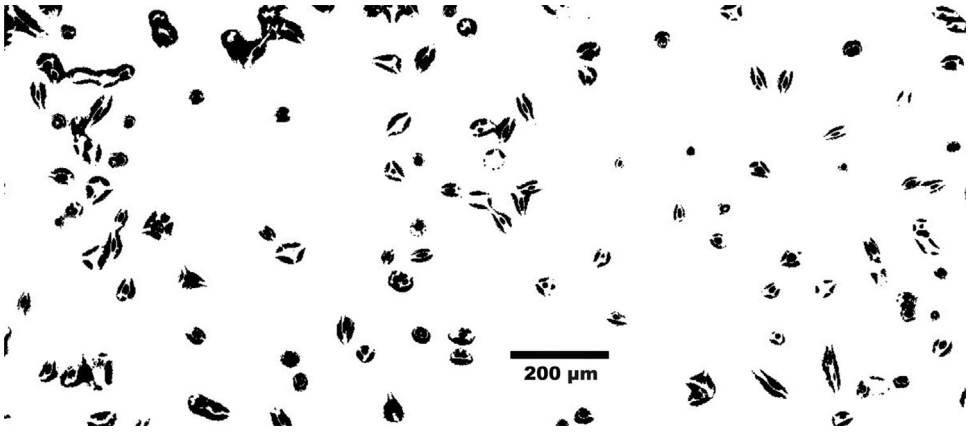

Fig. 2. Suboptimal segmentation using ImageJ (Schneider et al., 2012).

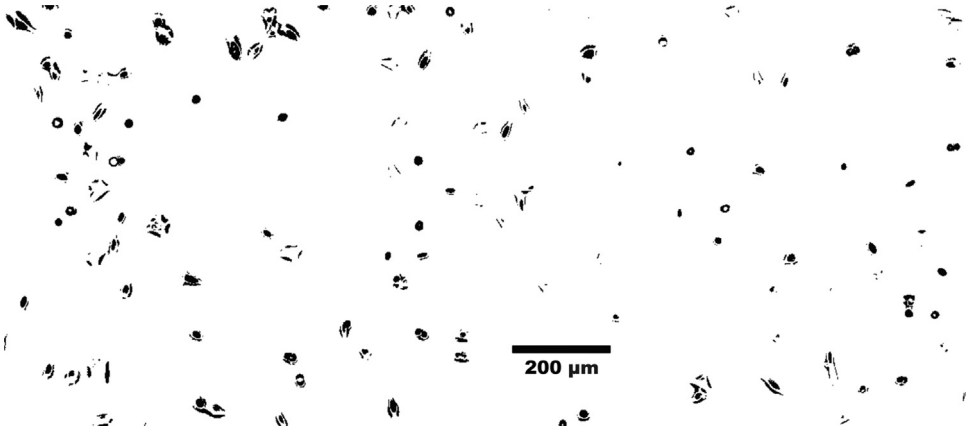

Fig. 3. Suboptimal segmentation from “Otsu” technique (Otsu, 1979) provided by ImageJ.

Table 1
Overview of existing cell tracking software/techniques (part 1/2).

Software/techniques	Features	Known drawbacks	Influential parameters and/or processes
Image registration cell tracking (Hand et al., 2009)	Combining both local average deviation in intensity (Zimmer et al., 2002), watershed (as segmentation) and image registration (which uses the first frame as the "landmark") to achieve cell detection and tracking.	The first frame has to be very accurately segmented otherwise errors may feed back to subsequent frames.	The segmentation on the first frame is the most influential parameter, others may include the range of background intensities (assumed to be low in Zimmer et al. (2002)).
Quimp2 (Bosgraaf et al., 2009)	Is able to detect cell positions and cell morphology, which then allows tracking movements of cell membranes. Segmentation is based upon cell edge detection using active contour method.	Manual selection of the cells is needed for the first frame.	It requires manual selection of the initial regions of cells and user-defined No. nodes used to represent the cell membrane.
Multi-target tracking (Li et al., 2008, 2006)	Using an interacting multiple models (IMM) motion filter in order to determine and learn the biological behaviour. The tracking is based on this IMM filter, thus requires algorithm training. Segmentation includes a geometric active contour via level-set and thresholding.	Is known to be problematic if cells overlap, and has extra training process.	Requires data from manual tracking where the ground truth is known to train the IMM filter.

Table 2
Overview of existing cell tracking software/techniques (part 2/2).

Software/techniques	Features	Known Drawbacks	Influential Parameters and/or Processes
3-D cell tracking (Rabut and Ellenberg, 2004)	Using 3-D image stack from fluorescent microscopy and some necessary thresholding to obtain cell position and outline. It uses the mass centre to locate the cell thus is accurate even when resolution is low.	Is only able to focus on one cell at a time, when multiple cells are present, each cell is visited sequentially. Manual selection of cells at the initial stage is required.	Initial manual selection is needed, threshold parameter is required to accurately obtain the cell outline.
Mitotic tree cell tracking (Debeir et al., 2005)	Using mean-shift tracking to detect cell positions and linking labelled cells with the nearest neighbour (on the subsequent frames). The proposed technique deals with artefacts (e.g. halos) from the phase-contrast images.	Manually tracking is required at the initial stage.	Manual selection is needed, parameters to identify the nearest neighbour is required, for example, the maximum distance a cell should search for.
Keyhole tracking (Reyes-Aldasoro et al., 2008)	A tracking algorithm to measure the velocity of red blood cells from fluorescent microscopy. Providing a trajectory, this algorithm is able to predict the next landing position of cells through a keyhole model. The cells are segmented using thresholding and a background reconstruction technique.	Due to the large quantity of data, image size may be reduced for efficiency.	The reconstruction of background is essential, threshold parameters are needed.

only aims to solve a subset of the whole problem. Some assumptions made by these techniques, seemingly appropriate to their specific problems, often prevent them from being integrated to solve other cell type problems. Hence it is vital to understand the pros and cons of each technique and their crucial assumptions if one wishes to extend these techniques to tackle other larger and more complex datasets. On the other hand, it would take an enormous effort to implement all techniques. Here we briefly summarise a number of the segmentation techniques in the literature.

Segmentation using image registration is proposed in Hand et al. (2009) for phase-contrast images. The technique Hand et al. used shows high accuracy in comparison to some of the other software packages. However, the use of registration requires the first frame to be segmented accurately in order to provide a "landmark" comparison to the subsequent frames. To automatically and accurately segment one image is arguably as hard as segmenting every image.

In the work of Debeir et al. presented in Debeir et al. (2005), their cell images also have halo artefacts and elongated features and their algorithm is capable of detecting proliferation and motility events. Their technique is based upon active contours, which means manually defining initial locations for the contours is required, and in particular, in their case, in the last frame of each video series. Also they assumed that the halo effect happens to every cell in their datasets.

Sezgin and Sankur (2004) have given a comprehensive survey on thresholding. They categorise thresholding methods into six groups based on the information they exploit. We refer the reader to their paper for a number of the local adaptive thresholding techniques.

Miura (2005) writes a detailed discussion on common tracking/segmentation techniques. In Table 1 on page 285 Miura summarises the pros and cons for the six common and classic techniques, apart from manual tracking and thresholding, they are Gaussian fitting, active contour, pattern matching and optical flow estimation. Gaussian fitting (Tardin et al., 1992) works with symmetric objects; active contour (Kass et al., 1988; Chan and Vese, 2001) requires the user to initially define the position of the "active contour", which means the user needs to manually track cells in one frame (typically the first frame). Local pattern matching (Gelles et al., 1988) needs objects with steady shape formation and finally optical flow estimation (Horn and Schunck, 1981) is sensitive to the changes in intensity.

Li et al. (2006) encounter many segmentation challenges similar to those in our dataset. For example, high enough cell density for frequent collisions and halo artefacts. In their work, they use a background subtraction followed by the "Otsu" thresholding technique for the segmentation. Then they apply a constrained level-set method to track each cell giving rise to good results. Inspired by this work, we have adapted some of their ideas to more efficiently and accurately deal with cell detection with the key features of our approaches summarised in this article. It must

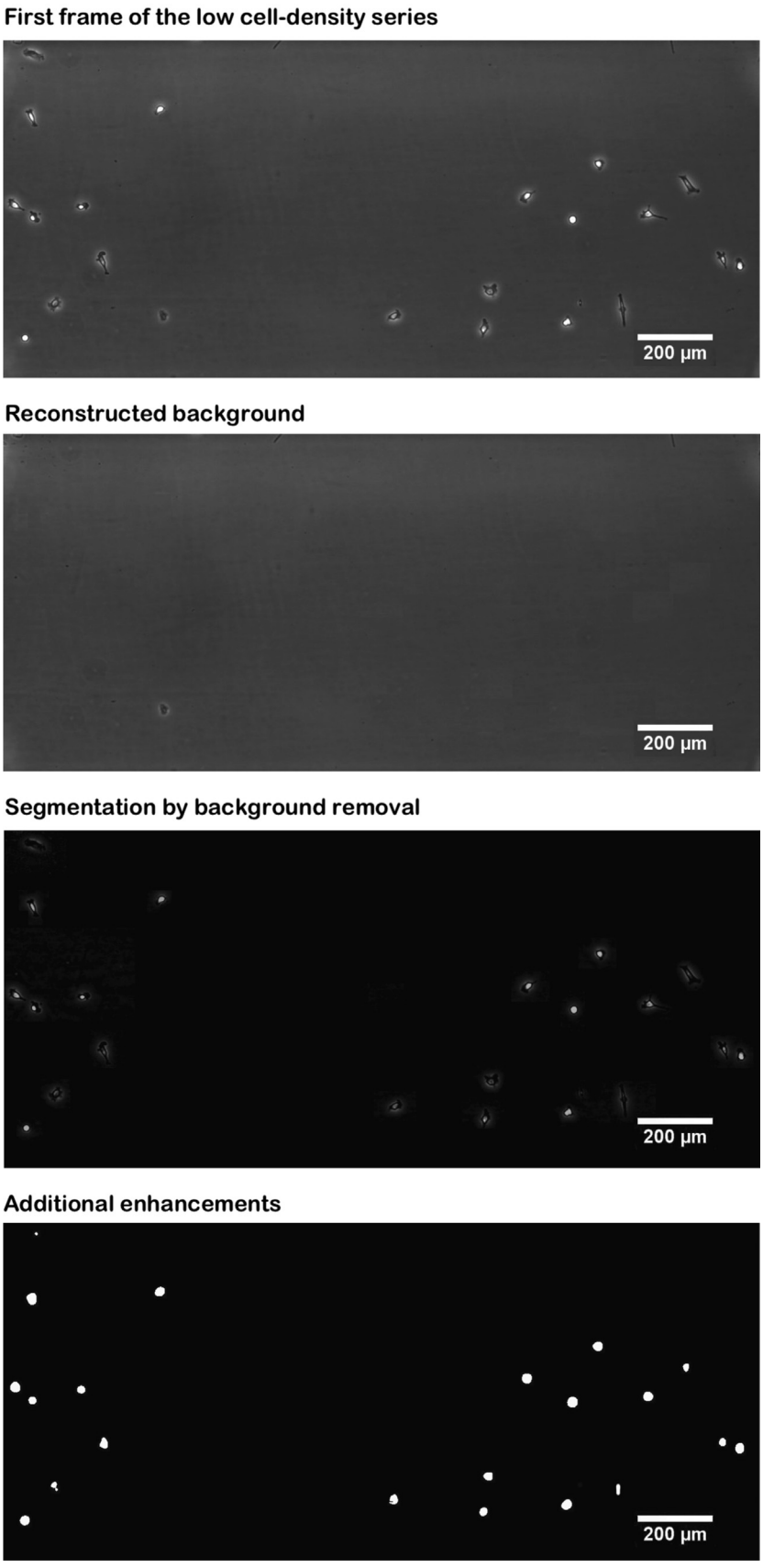

Fig. 4. Background reconstruction and removal (Xiao et al., 2012) in a low cell-density series.

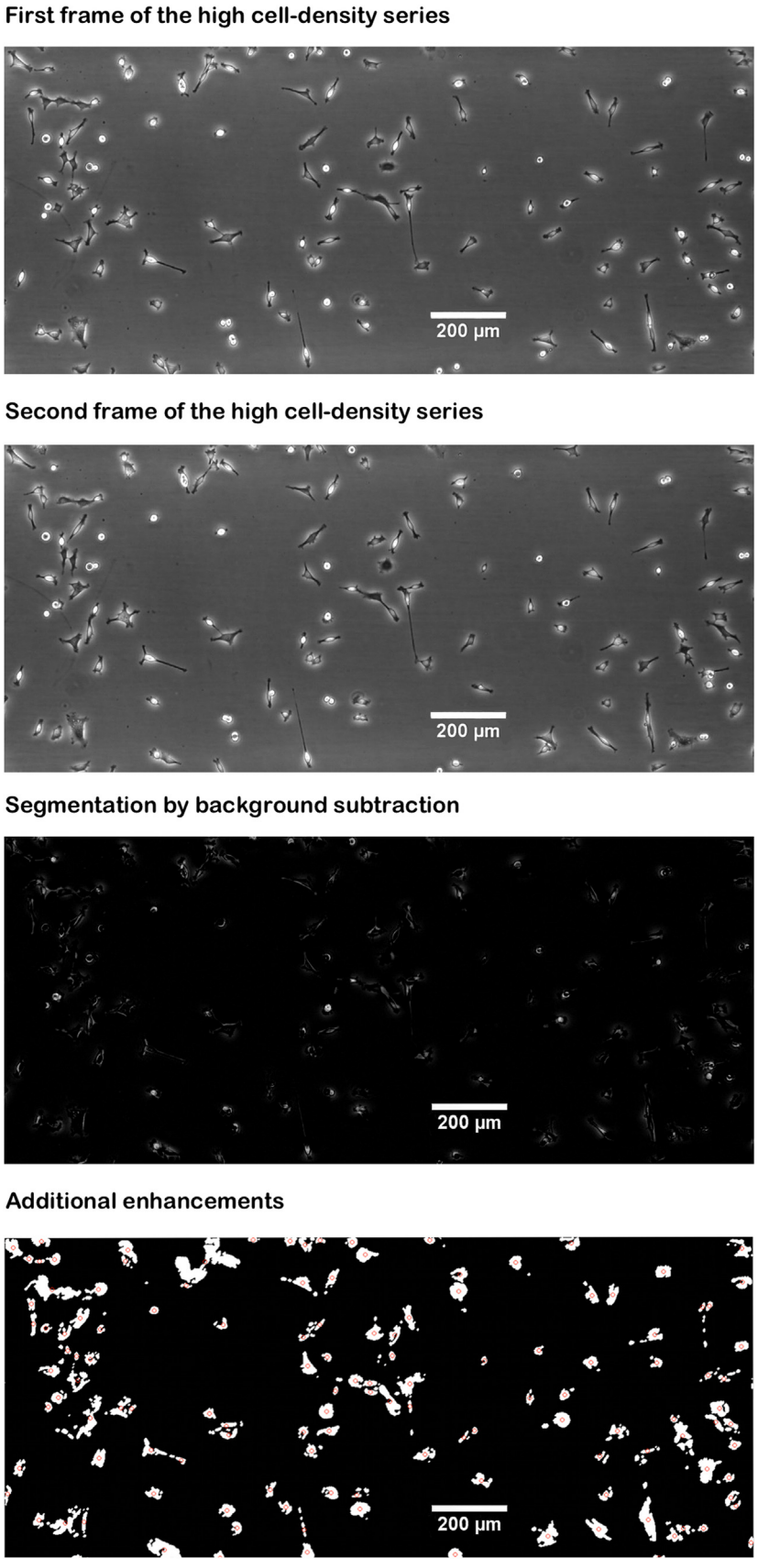

Fig. 5. Our segmentation technique based on the background subtraction (Xiao et al., 2012) in a HCD series. In the last picture, each identified cell is marked with a red circle. (For interpretation of the references to colour in this figure caption, the reader is referred to the web version of this paper.)

be noted that their datasets are phase-contrast microscopy images and they assume a uniform background intensity and their constrained level-sets prevent whole cells overlapping. We refer the reader to Li et al. (2008) for a more detailed summary of their work. We also would like to bring to the attention of the reader the fact that there are many segmentation techniques in other fields such as cancer image analysis (Reyes-Aldasoro et al., 2010) and optical remote sensing (Dey et al., 2010), which might provide useful ideas for these kind of datasets.

In Tables 1 and 2 we briefly summarise some current software and techniques; we detail their important features and drawbacks and comment on their most influential parameters/processes.

3.2. Segmentation via background reconstruction

Inspired by the so-called background reconstruction and subtraction techniques from Li et al. (2006), Reyes-Aldasoro et al. (2008), and Xiao et al. (2012), we propose a methodology in order to deal with the datasets such as those considered in this work.

3.2.1. Low-cell-density data

In order to proceed with clarity, for illustrative purposes, we present our background reconstruction algorithm for the case of a low-cell-density (LCD) dataset. We make two assumptions about the data:

- background intensity between frames is constant or has very small variation,
- the position of the camera relative to the substrate is fixed, so the movements of the cells are not from the drift (e.g. vibration) of the equipment.

To reconstruct the background, we take the mode of the intensity value occurring in all frames at each pixel. Due to the fact that cells are generally moving around (hence the need for tracking), and the density is low, the mode value at each pixel is most likely to be the intensity of the background or a stationary noise that we would categorise as background as well. In Fig. 4, we illustrate this idea with a dataset of LCD images. Fig. 4 consists of four images; in the first we display the first frame of the original dataset, in the second we display the reconstructed background, in the third we display the first image with the reconstructed background removed and in the fourth we display the binary image that is obtained from the grey-scale image shown in the third row.

After having the background reconstructed, all frames can be subtracted from it, and whatever the differences are, these are either moving cells or simply noise. We can then separate the cells by their areas and/or trajectories following a common identification procedure (Li et al., 2008; Meijering et al., 2012).

3.2.2. Higher-cell-density data

Having discussed segmentation in a LCD situation, here we focus on datasets which often have higher number of cells. Note that these higher-cell-density (HCD) situations usually have approximately around 15–30% confluences in the field of view (Topman et al., 2011). This is because a sufficient number of cells is required to determine cell behaviour, but there must be enough room for cell migration.

Reconstruction of the background is more difficult in the HCD situations, meaning cell collisions and overlaps happen very often. Some parts of the background may not be exposed throughout the whole experiment.

To provide a solution, we take the differences between consecutive frames, and by assuming a steady background with near-constant intensity, we can remove the background in the resulting image. The differences between these two images indicate what has moved or what intensity has changed in this time interval. This is demonstrated in the first three pictures in Fig. 5. Note that since we are using background subtraction, we no longer need to reconstruct the background.

3.2.3. Obtaining cell centroids from the segmented data

Having subtracted the background and obtained an image with potential candidates of cells, the next step is to determine the centroids of cells and filtering out those that are not cells. A user-defined threshold parameter is included for the size of particles, and we rule out those very small ones that are most likely to be noise. This is a common approach and was used in Gal and Weihs (2012) and Crocker and Grier (1996). In the example presented here, our choice of the threshold parameter is equal to 75, meaning connected regions that have less than 75 non-zero pixels are discarded.

An additional challenge in the HCD situations is to separate or remove collided cells which this is not a trivial task. Algorithms described by Crocker and Grier (1996) and Gal and Weihs (2012) have been looking at how to determine individual candidates (cells or particles) from a collision. In both algorithms, the brightest pixels in the image are identified as potential confidantes. Crocker and Grier relied on circles with a user-defined size to surround each candidate. Gal and Weihs subsequently improved on this by using a "blob analysis" which only keep circles that are bright enough, within a user-specified size range and exhibit a minimal eccentricity.

On the other hand, in our situation, we are unable to identify candidates using their intensity (for example, in Fig. 1, arrow b points to cells that do not have a bright centre) nor by a set of circles with a uniform size (for instance, arrow c points to cells that would have very different sizes if they are surrounded by circles).

After the background is subtracted, we apply erosion and dilation techniques (Miura, 2005). These are averaging processes; the erosion aims to create gaps when candidates are linked with narrow "bridges" and the dilation is used to link each cluster of smaller pieces together. How much we average is controlled by given parameters and requires either preliminary knowledge about the image or by training the software with numerous datasets. However, the number of iterations for the erosion is

Table 3
Summary of the centroid counts from our segmentation technique on one particular dataset.

Frames	Centroids	Frames	Centroids	Frames	Centroids
2	130	26	133	50	125
3	131	27	127	51	126
4	122	28	132	52	118
5	121	29	124	53	117
6	119	30	131	54	119
7	122	31	138	55	116
8	126	32	137	56	116
9	128	33	127	57	117
10	112	34	136	58	123
11	123	35	131	59	121
12	125	36	129	60	119
13	136	37	119	61	118
14	136	38	130	62	117
15	122	39	129	63	124
16	133	40	127	64	119
17	120	41	141	65	126
18	134	42	126	66	122
19	124	43	129	67	115
20	127	44	129	68	121
21	133	45	123	69	115
22	132	46	125	70	117
23	126	47	124	71	118
24	136	48	129		
25	136	49	119		

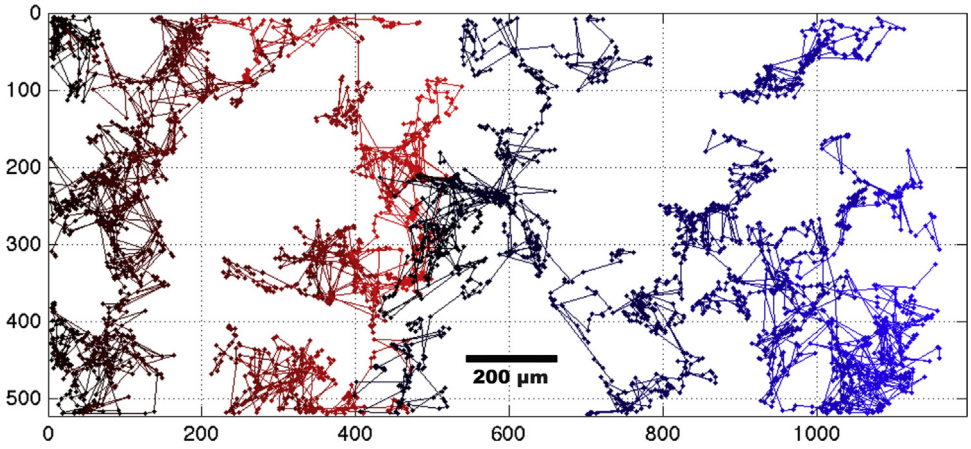

Fig. 6. Our particle tracking results. Note that 61 distinct persistent trajectories are shown in the above plot and each trajectory is marked with a distinguishable (by computer) colour from the others. (For interpretation of the references to colour in this figure caption, the reader is referred to the web version of this paper.)

always larger than the one for the dilation. In the example presented here, we take 15 iterations of the erosion and 10 iterations of the dilation.

After these segmentation techniques, the image is reduced to binary where 1 represents cells and 0 represents background. The centroid of each connected region is the centre of that area. The last picture in Fig. 4 illustrates our segmentation. Segmentations for the full length of the video (*Segmented.avi*) is included in the supplementary materials.

The segmentation shown in Fig. 5 is calculated using the first and the second frames of a particular dataset. We present some statistics of the segmentation for the whole dataset (72 frames in total) in Table 3. Note that we always subtract frame 1 from frame 2 to start with, thus in the table, the illustration begins from frame 2.

3.3. Particle tracking

Having obtained usable segmentation images, particle tracking is relatively straightforward. It basically links particles between consecutive frames and due to the segmentation which generally is quite "brutal", there is limited information a tracking algorithm can use.

Sbalzarini and Koumoutsakos (2005) proposed a feature point tracking algorithm which takes into account the various intensity values of the cells and the backgrounds. Rabut and Ellenberg (2004) used a 2-D projection technique to achieve 3-D singe cell tracking.

3.3.1. Methodology and results of particle tracking

The particle tracking method we follow is a straightforward nearest-neighbour approach where particles between frames are linked to their nearest neighbours (Crocker and Grier, 1996; Hand et al., 2009). We also prevent links which are considered to be biologically implausible (i.e. above the maximum distance a cell can travel in a given time interval). Our software framework, **DotConn**, combines the segmentation described in Section 3.2 and particle tracking. It is written in Matlab with the use of its Imaging Processing Toolbox (Gonzalez et al., 2004).

Here we describe our particle matching and tracking in detail. Assuming two input datasets from two segmentations, $A(\vec{c}_A)$ and $B(\vec{c}_B)$, with N_A and N_B the total number of centroids in datasets A and B respectively and with $\vec{c}_A = \{\vec{c}_{A,i}\}, i = 1, \ldots, N_A$ and $\vec{c}_B = \{\vec{c}_{B,j}\}, j = 1, \ldots, N_B$ the positions of each centroid. We define a threshold distance $D > 0$ such that links between centroids whose distance from each other is greater than D is considered implausible. Our linking procedure is defined as follows, first we compute an $N_A \times N_B$ array whose $\vec{d}$ entries are given by the Euclidean distance between the i^{th} centroid in dataset A and the j^{th} centroid in dataset B

$$d_{i,j} = |\vec{c}_{Ai} - \vec{c}_{Bj}|. \quad (1)$$

We create a link between the centroids $\vec{c}_{A,i^*}$ and $\vec{c}_{B,j^*}$ which minimise the above distance. We then remove the distances associated with the linked $\vec{c}_{A,i^*}$ and $\vec{c}_{B,j^*}$, i.e., the i^*th row and j^*th column of $\vec{d}$, and apply the above procedure recursively (i.e., create a link corresponding to the minimum entry of the remaining $(N_A - 1) \times (N_B - 1)$ array of distances) until either the $\min_{i,j} d_{i,j} > D$ or all the cells in either dataset A or B have been linked. In the example dataset whose first and second frames are shown in Fig. 5, our choice of D is 50 pixels per frame as the Euclidean distance (roughly around 83 μm).

In order to aid robustness in practice, we allow centroids that have not been matched to search backwards with up to three previous frames. This proves crucial in dealing with difficulties, for example, when cells collide.

Table 4
Summary of the matching procedure from our particle tracking technique on one particular dataset. The abbreviation "F.F.P.F" means "found from the previous frame".

Frames	Cells	F.F.P.F	Frames	Cells	F.F.P.F	Frames	Cells	F.F.P.F
2	130	–	26	133	131	50	119	116
3	131	130	27	127	125	51	125	114
4	122	121	28	132	124	52	126	124
5	121	120	29	124	122	53	118	118
6	119	118	30	131	120	54	117	116
7	122	117	31	138	124	55	119	115
8	126	118	32	137	137	56	116	116
9	128	124	33	127	125	57	116	115
10	112	112	34	136	123	58	117	114
11	123	107	35	131	129	59	123	109
12	125	122	36	129	129	60	121	120
13	136	118	37	119	118	61	119	118
14	136	135	38	119	118	62	118	118
15	122	120	39	130	113	63	117	115
16	133	119	40	129	129	64	124	110
17	120	120	41	127	127	65	119	119
18	134	106	42	141	116	66	126	113
19	124	123	43	126	124	67	122	121
20	127	122	44	129	125	68	115	115
21	133	123	45	129	129	69	121	110
22	132	132	46	123	121	70	115	114
23	126	124	47	125	122	71	117	112
24	136	119	48	124	121	72	118	115
25	136	135	49	129	122			

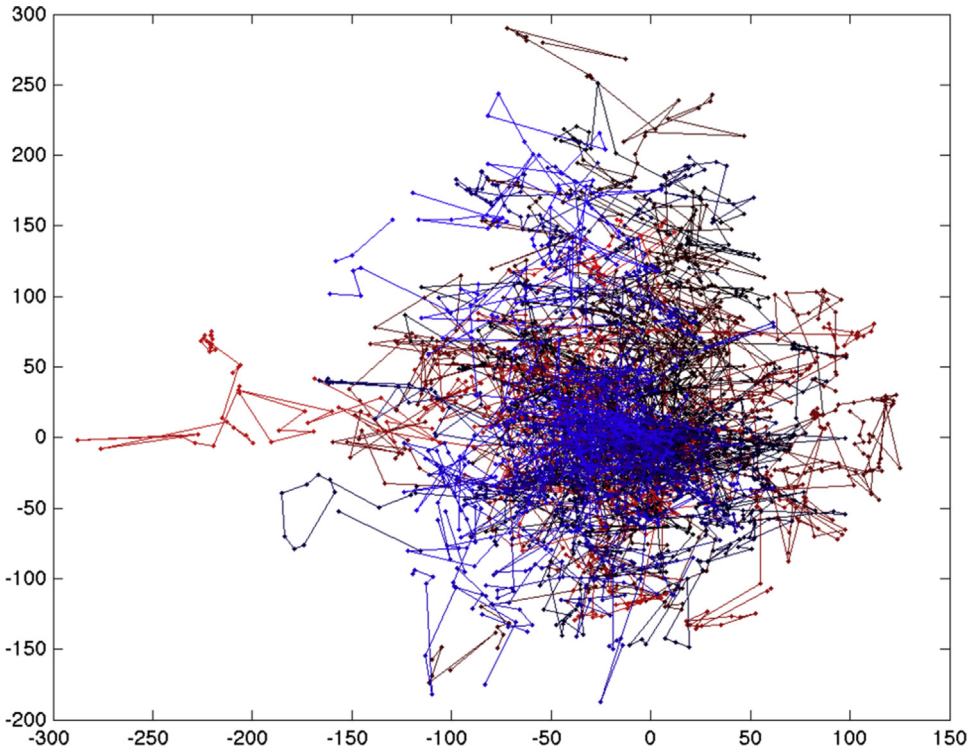

Fig. 7. The spider plot from our tracking result shown in Fig. 6.

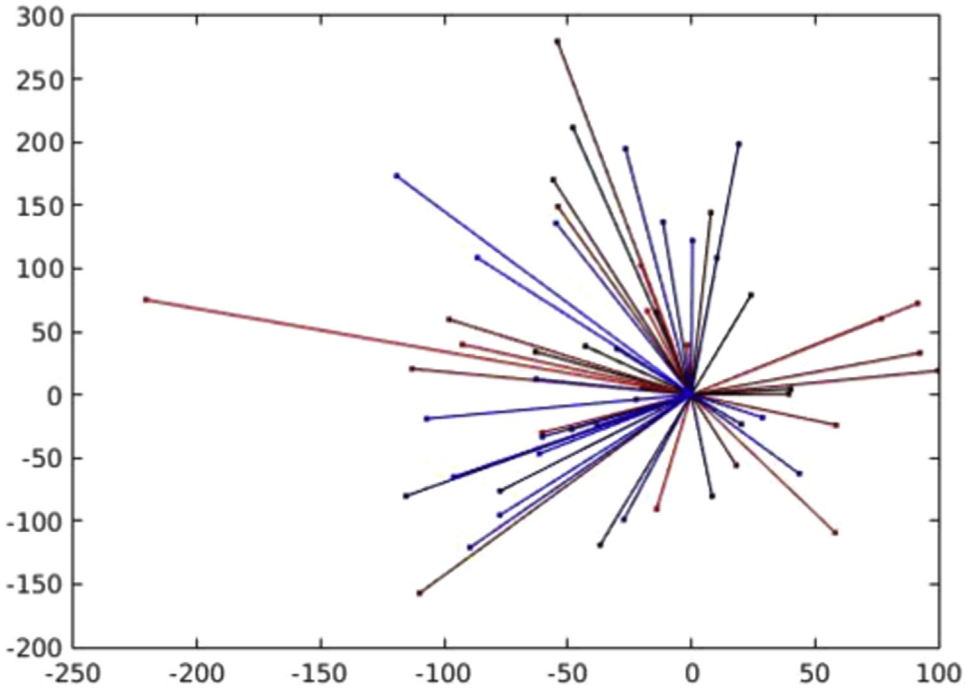

Fig. 8. The star plot from our tracking result shown in Fig. 6.

An extra complication from the dataset is that cells move freely in and out of the field of view. Therefore, the number of cells in an experiment will increase (or decrease) as time goes by. For cells moving in, we assume that it is a new cell that has moved in. This can be problematic if we want to summarise the tracking information. To simplify the matter, we focus on persistent cells which we define as those cells that appear in 90% of all the frames (due to frequent collisions and overlapping, we cannot assume 100% identification). The particle tracking results from our approach are illustrated in Fig. 6 where only the persistent cells are shown. In Table 4 we present the number of cells in each frame of a given dataset (consisting of 72 frames) together with the number of cells from the previous frame.

Although the choice presented here is the nearest-neighbour approach, we refer the interested reader to Meijering et al. (2012) where Meijering et al. summarized a dozen measurements that can be obtained with just centroid positions. For example, one may compute the instantaneous angle (between two centroids that is

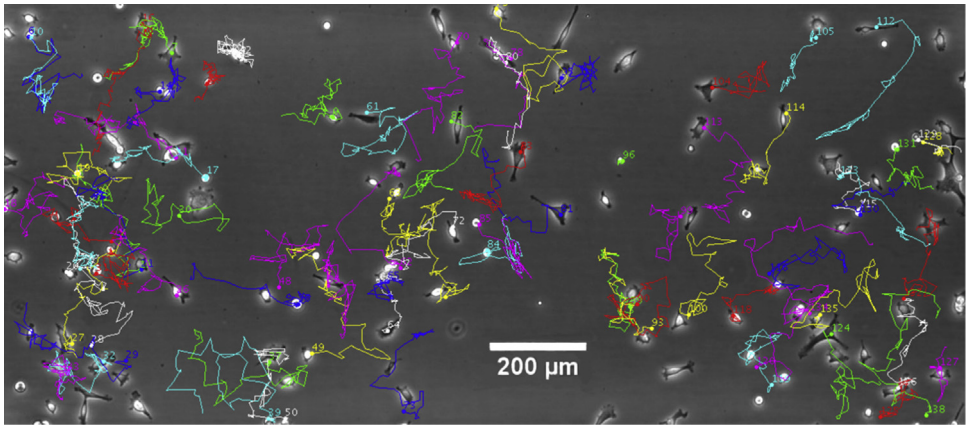

Fig. 9. Results from manual tracking.

relative to the chosen axis direction), directional change (from two consecutive angles) and instantaneous speed (given time and spatial units). This information could be essential to improve the particle tracking if the behaviour of the current type of cells are well understood, say if the maximum degree of directional change (within a certain time interval) is known, then the particle tracking may rule out those that violate this biological theory.

In order to graphically depict whether cells exhibit directed migration, here we use two different plots: one is the so-called spider plot, where the complete set of trajectories is used; the other is the so-called star plot, where only the starting and ending positions are included. The spider plot is shown in Fig. 7; it is produced by translating the linked trajectories, shown in Fig. 6, such that the starting point of each trajectory is the origin. The

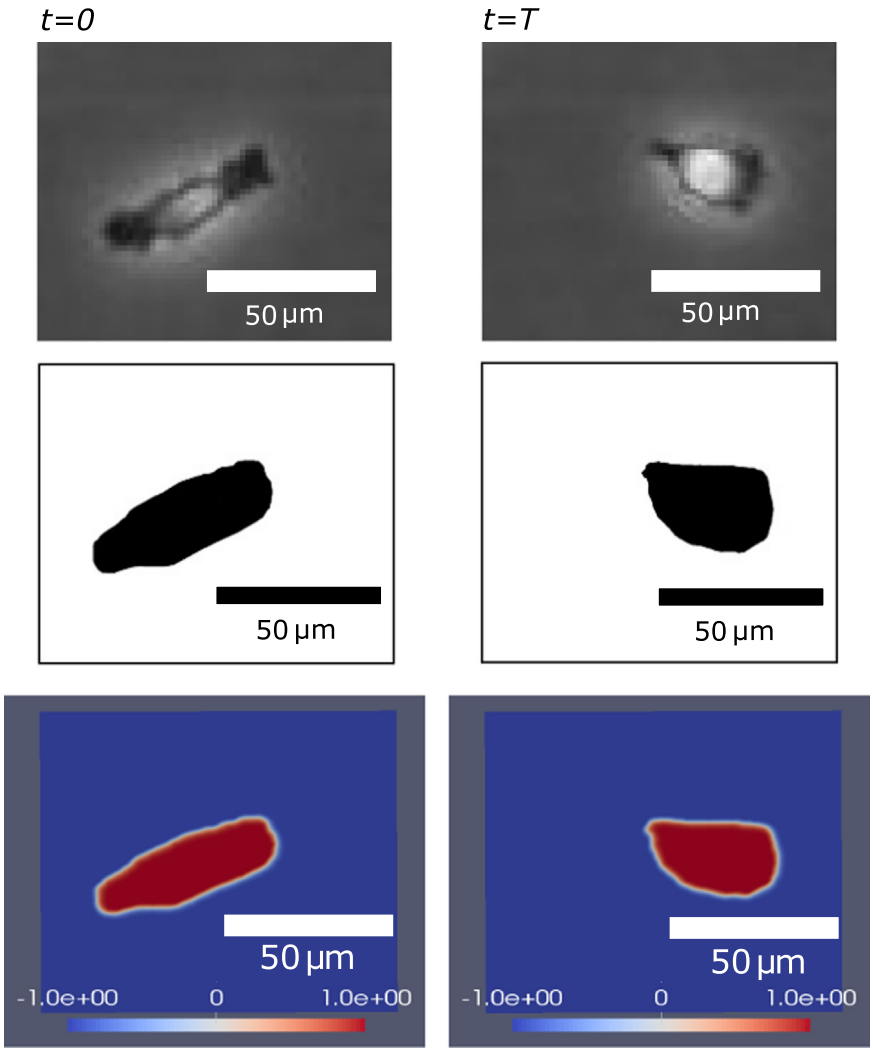

Fig. 10. Cell one, first row: frames from data; second row: segmentation; third row: phase-field representations.

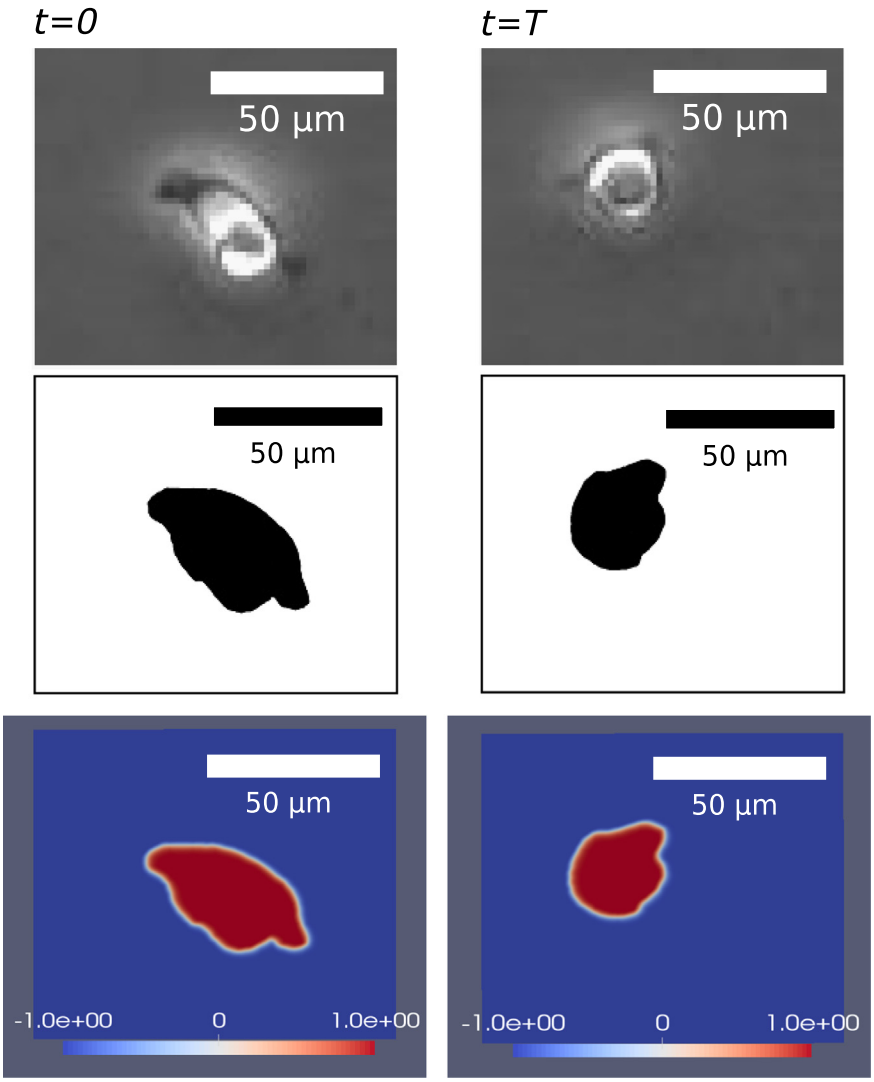

Fig. 11. Cell two, first row: frames from data; second row: segmentation; third row: phase-field representations.

spider plot has information in the transition but may be unclear when the number of cells is large. Thus the star plot is employed and shown in Fig. 8, a straight line links the translated starting position (the origin) to the end position of each trajectory. From the two plots, we observe no clear directional bias with trajectories evenly distributed over 360°, which is as expected since as outlined in Section 2, the current dataset is obtained from an experiment performed without a chemoattractant.

For the purpose of validation, we also performed manual tracking on the dataset, using a package provided by ibidi GmbH in ImageJ the result of which is shown in Fig. 9. Using the manual tracking tool, the first frame has 140 cells, while using **DotConn**, we found 130 cells. There are 63 persistent cells from manual tracking and our software gives 61. A full length video of the results of manual tracking (*manual_tracking.avi*) is included in the supplementary materials.

4. Whole cell tracking through the optimal control of geometric evolution laws

In this section we broaden the focus from tracking cell centroids to tracking whole cell morphologies with the goal of recovering morphological dynamics. Some of the previously mentioned segmentation techniques also belong to this category, for example, the use of active contours (Debeir et al., 2005; Kass et al., 1988; Chan and Vese, 2001), level-set methods (Li et al., 2008, 2006; Mosaliganti et al., 2013) and the optical flow estimation described in Miura (2005). Recent work from Bosgraaf et al. (2009) suggests the use of local membrane displacement based upon the active contour method (Kass et al., 1988) to track and linearly interpolate movements of cell membrane.

Our current research on whole cell tracking is an extension of the work described in Haußer et al. (2010) and Haußer et al. (2012). The aim is to determine trajectories of points on the cell boundary from position A at time 0 to position B observed at time T.

Mathematically, we formulate this problem as an optimal control problem as in Blazakis et al. (2015), where we propose that the evolution of the cell shape follows a volume constrained forced mean curvature flow (VCMCF). We consider the phase-field or diffuse interface approximation of the VCMCF given by the mass constrained Allen-Cahn equation with forcing η (see for example Brassel and Bretin, 2011),

$$\epsilon\frac{\partial}{\partial t}\phi(\vec{x},t)=\epsilon\Delta\phi(\vec{x},t)-\epsilon^{-1}G'(\phi(\vec{x},t))+\eta(\vec{x},t)+\lambda(t)\ \text{in}\ \Omega\times(0,T], \tag{2}$$

$$\phi(\vec{x},0)=\phi^0(\vec{x})\ \text{in}\ \Omega, \tag{3}$$

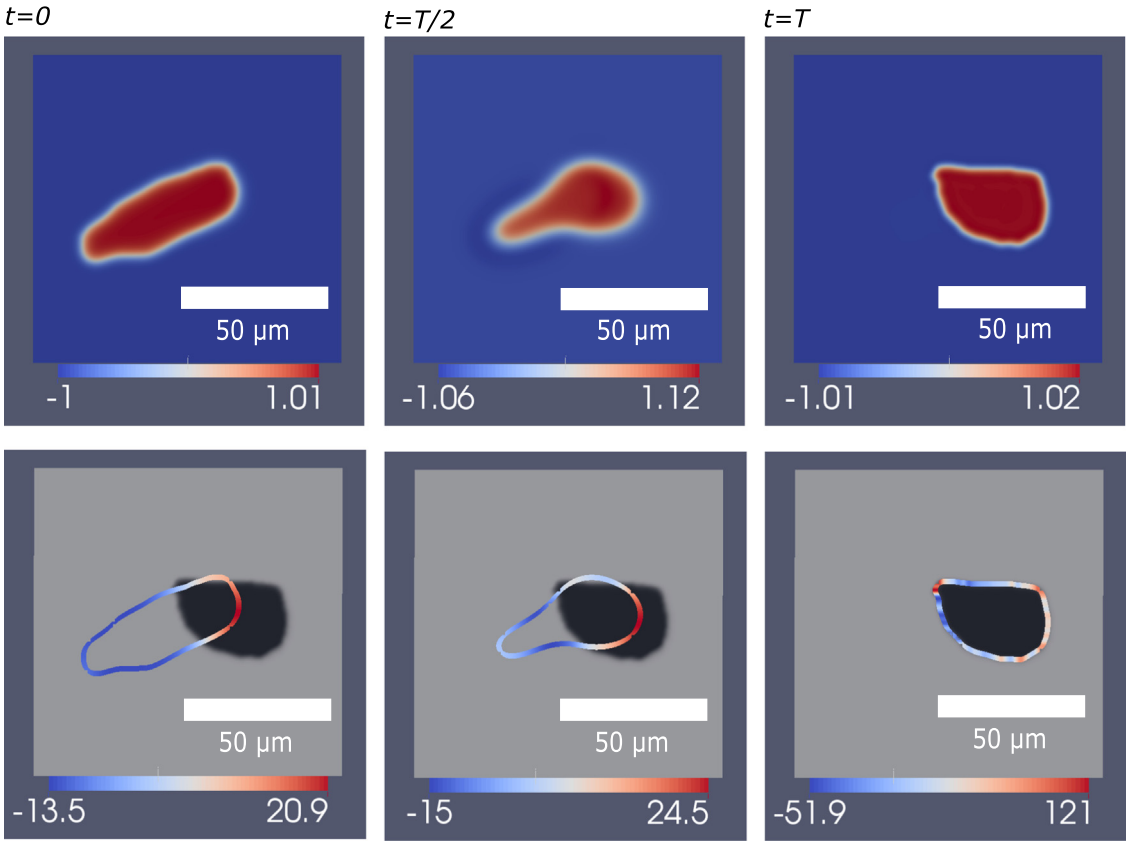

Fig. 12. Cell one, first row: solutions of the phase-field variable ϕ; second row: values of the computed optimal control η^* on the zero isosurface of ϕ, the background is coloured by the diffuse interface representation of the desired shape. (For interpretation of the references to colour in this figure caption, the reader is referred to the web version of this paper.)

$$\nabla\phi(\vec{x},t)\cdot\vec{\nu}_{\Omega}(\vec{x})=0 \quad \text{on} \quad \partial\Omega, \tag{4}$$

where $\phi(\vec{x},t)$ is a phase-field variable that takes the value approximately $+1$ inside $\Gamma_\epsilon(t)$ and approximately -1 outside $\Gamma_\epsilon(t)$ where Γ_ϵ is a diffuse interface approximation of the $d-1$ dimensional cell boundary $\Gamma(t)$. The *time independent* domain $\Omega \subset \mathcal{R}^d$ is a bounded domain that contains $\Gamma_\epsilon(t)$ for all $t\in[0,T]$, $\epsilon>0$ governs the interfacial width of the diffuse interface $\Gamma_\epsilon(t)$, $G(\phi)=\frac{1}{4}(1-\phi^2)^2$ is a double well potential which has minima at ± 1 and λ is a time-dependent constraint on the mass that models a volume constraint (see Blazakis et al. (2015), Blowey and Elliott (1993), and Yang et al. (2015) for more details) and $\vec{\nu}_{\Omega}$ is the normal to $\partial\Omega$.

It is worth noting that in general, the volumes enclosed by the target and initial interfaces may differ, i.e., $\int_\Omega \phi^0 \neq \int_\Omega \phi_{obs}$ and so enforcing a volume constraint of the initial mass is inappropriate, instead we proceed as in Blazakis et al. (2015) and define $M_\phi(t)$, the linear interpolant of the mass of the initial and target diffusive interfaces by

$$M_\phi(t) := \int_\Omega \left[\phi^0(\vec{x})+\frac{t}{T}\left(\phi_{obs}(\vec{x})-\phi^0(\vec{x})\right)\right]. \tag{5}$$

The volume constraint $\lambda(t)$ in (4) is then determined such that for $t\in(0,T]$

$$\int_\Omega \phi(\vec{x},t)=M_\phi(t). \tag{6}$$

In order to formulate our optimal control problem we introduce the objective functional J, which we seek to minimise

$$J(\phi,\eta)=\frac{1}{2}\int_\Omega\left(\phi(\vec{x},T)-\phi_{obs}(\vec{x})\right)^2 d\vec{x}+\frac{\theta}{2}\int_0^T\int_\Omega \eta^2(\vec{x},t)\,d\vec{x}\,dt, \tag{7}$$

where $\theta>0$ is a regularisation parameter. The first term of the right-hand side of (7) is the so-called fidelity term which measures the distance between the solution of the model and the target dataset ϕ_{obs} and the second term is the regularisation which is necessary to ensure a well-posed problem (Tröltzsch, 2010).

The optimal control problem we consider in this work may now be stated as the following minimisation problem. Given initial data ϕ^0 and target dataset ϕ_{obs}, find a space-time distributed forcing $\eta^*:\Omega\times[0,T)\to\mathcal{R}$ such that with ϕ a solution of (4) with initial condition $\phi(\cdot,0)=\phi^0(\cdot)$, the forcing η^* solves the minimisation problem

$$\min_\eta J(\phi,\eta), \text{ with } J \text{ given by } (7). \tag{8}$$

In Blazakis et al. (2015) and Yang et al. (2015) we have formally derived the first order optimality conditions associated with the above optimal control problem. Specifically, a gradient-based iterative update of the control η is employed with the use of a Lagrange multiplier. Furthermore, we propose and implement an efficient adjoint based numerical method for its approximation. We refer the interested reader to the aforementioned references for further details.

We present results obtained using the algorithms in Yang et al. (2015) applied to two single cells, cell one and cell two, from the dataset. The two cells are presented in Figs. 10 and 11 respectively. In both figures, the first rows display the actual images, the second rows display the segmentation and the third rows display the phase-field representations of the cells. The full length videos (*cell_one.avi* and *cell_two.avi* respectively) are included in the supplementary materials. The accuracy of this morphological identification is relatively high, this is because after zooming in to a single cell, the background is relatively

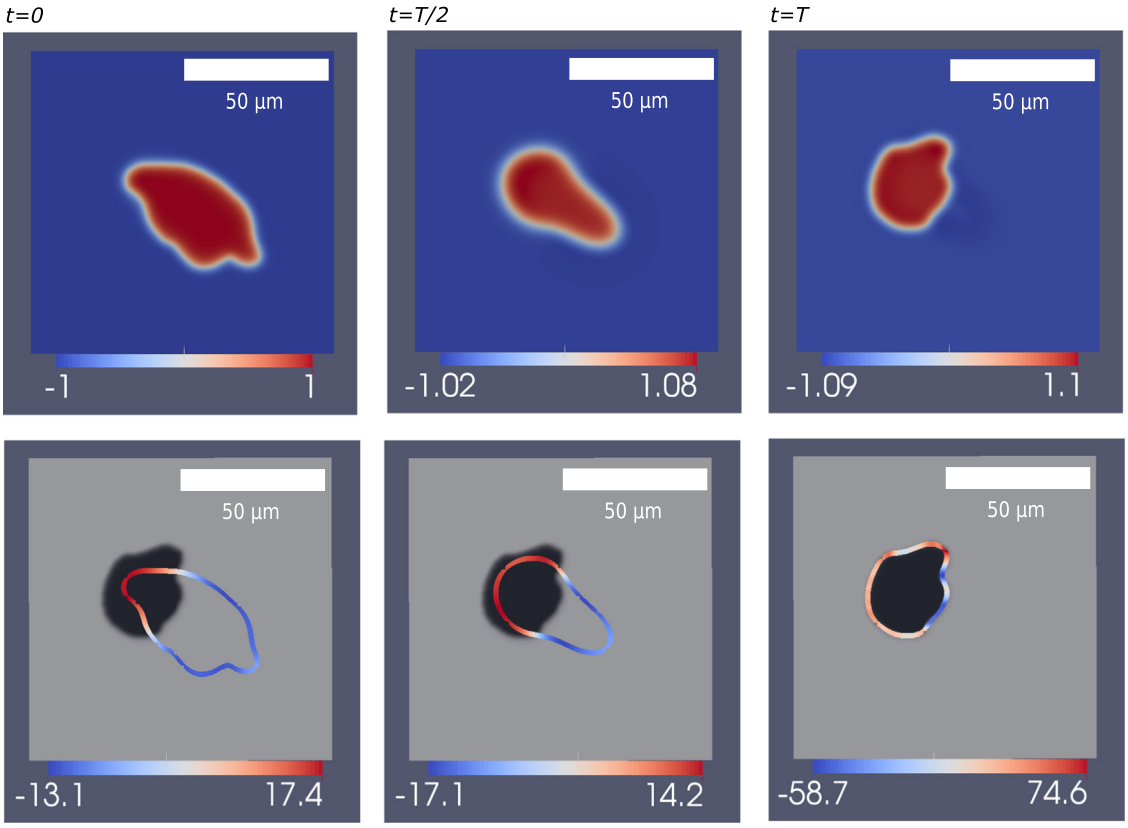

Fig. 13. Cell two, first row: solutions of the phase-field variable ϕ; second row: values of the computed optimal control η^* on the zero isosurface of ϕ, the background is coloured by the diffuse interface representation of the desired shape. (For interpretation of the references to colour in this figure caption, the reader is referred to the web version of this paper.)

homogeneous. The segmentations presented in the second rows of both figures are from an edge detection algorithm which is based upon changes in intensity described in Sacan et al. (2008) followed by the "Otsu" thresholding (Otsu, 1979). Both algorithms have been commonly used, see for example, (Li et al., 2008, 2006; Rabut and Ellenberg, 2004; Debeir et al., 2005; Reyes-Aldasoro et al., 2008).

We show the solutions at the very first time step, halfway through and the final time computed with the optimal control η^* in Figs. 12 and 13 for cells one and two respectively. We see good correspondence between the desired and computed shapes at the final time whilst the intermediate shapes resemble polarised cells with the computed forcing η^* clearly illustrating protrusive forces concentrated near the front of the cell with contractile forces at the cell rear.

The accuracy of our model is generally influenced by, first, the segmentation techniques. Although we mentioned that it is relatively easy to segment a single cell once one has zoomed in, the segmentation may still be affected by artefacts like the halos. Furthermore, the resolution of the original image generally defines the starting point of the computational resolution (i.e. degrees of freedom) and thus undoubtedly contributes to the overall accuracy. Finally, with respect to the phase-field modelling, the smaller ϵ is, the narrower the diffuse interface (between 1 and -1) will be, thus the more accurate the approximation along the cell membrane is going to be. However, a small ϵ requires the use of very fine meshes, and this prolongs the computation. Hence an efficient solver with advanced computational techniques as well as state-of-the-art algorithms is needed. We direct the interested reader to Blazakis et al. (2015) and Yang et al. (2015) for further details. The choice of ϵ in the presented examples is 0.1 with an arbitrary domain size of 0–1. Note that the physical model is the VCMCF which is obtained in the limit $\epsilon \to 0$ of the phase-field model. Hence ϵ can be seen as another regularisation parameter just like θ and should be taken as small as is feasible.

As the recovered morphologies are obtained by fitting a model, derived from physical principles, to the data, the physical features present in the model are reflected in the recovered morphologies. To illustrate this we report on the mass ($\int_\Omega \phi \, d\vec{x}$) and volume ($\int_{\{\phi>0\}} 1 \, d\vec{x}$) of our recovered cell morphologies. It is worth noting that

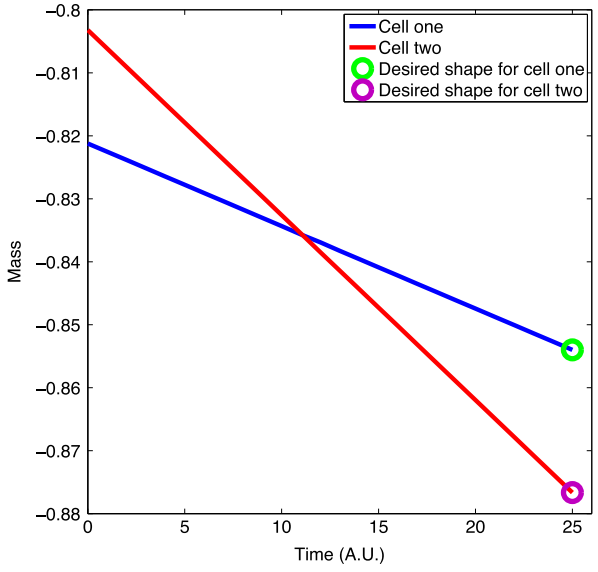

Fig. 14. Non-physical mass ($\int_\Omega \phi \, d\vec{x}$) of the observed and reconstructed morphologies of cells one and two.

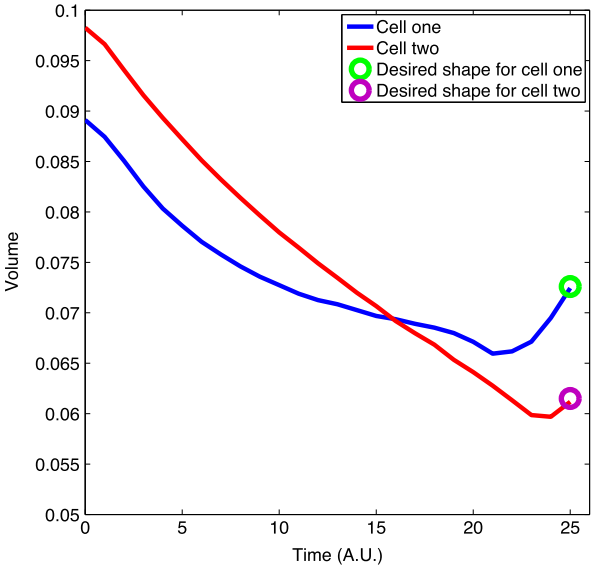

Fig. 15. Area of the positive phase ($\int_{\{\phi>0\}} 1\, d\vec{x}$) of the observed and reconstructed morphologies of cells one and two.

since we use the phase-field representation, the phase-field variable ϕ takes values approximately in the range between $+1$ and -1. Therefore, the reported mass obtained through $\int_{\Omega}\phi\, d\vec{x}$ may be a negative value. This is because the area of the background ($\phi \approx -1$) could be larger than the area of cells. We advise the reader to see the mass as a non-physical but numerical measurement. On the other hand, the volume which is computed through $\int_{\{\phi>0\}} 1\, d\vec{x}$, is a physical approximation to the cell volume.

The evolution of the (non-physical) mass is shown in Fig. 14 and the volume in Fig. 15. We recall that our model approximates the constraint on the mass of the order parameter ϕ. This is evident in Fig. 14 where we see the mass is exactly at the desired value (note that we do not enforce conservation to a constant mass as the mass of the initial and target data differ, rather we constrain to the linear interpolant of the mass). The resulting volume, i.e., diffuse interface approximation of the cell area, shown in Fig. 15 whilst not exact is nonetheless close to being the linear interpolant of the initial and desired volume. In particular it is clear that we do not observe artefacts such as large losses or gains in volume during the evolution which we would otherwise expect to see without the inclusion of mass constraint.

5. Conclusion

In this work, we present two frameworks for cell tracking. The first is based upon detection where cells are represented by dots via segmentation of phase-contrast microscopy images. Then dots are linked between time frames to create cell trajectories. We demonstrated the performance of our software **DotConn** on an example experimental dataset. Initial comparisons of our algorithm with manual tracking suggests that our framework is able to produce satisfactory results. Secondly we proposed an algorithm for whole cell tracking based on fitting a mathematical model for the evolution to the data. An advantage of the proposed approach is that the physics of the model are reflected in the recovered morphologies.

There are many possible directions for future research. Clearly more tests of the robustness of our algorithms with different datasets is warranted. We believe our segmentation can be further improved by looking at some sophisticated techniques, such as the region-aided geometric snake (Xie and Mirmehdi, 2004) and advanced local thresholding (Sezgin and Sankur, 2004). Referring back to the second assumption made in Section 3.2.1 about the images, it is possible to deal with the drift of equipment by including image registration techniques. In terms of the approach for whole cell tracking, we wish to build in additional biological constraints so that the reconstructed cell movements reflect more realistic biological assumptions/hypotheses. For example, the mechanics of the interior of the cell plays an important role in the evolution of cell shape and this is something we wish to include in future work.

Conflict of interest statement

None declared.

Acknowledgement

FY, CV, VS and AM acknowledge support from the Leverhulme Trust Research Project Grant (RPG-2014-149). The work of CV, VS and AM was partially supported by the Engineering and Physical Sciences Research Council, UK grant (EP/J016780/1). This work (AM, ZG, EH, RZ) has also received funding from the European Union's Horizon 2020 research and innovation programme under the Marie Sklodowska-Curie grant agreement No 642866. The work of CV is partially supported by an EPSRC Impact Accelerator Account award. This research was finalised whilst all authors were participants in the Isaac Newton Institute Program, Coupling Geometric PDEs with Physics for Cell Morphology, Motility and Pattern Formation. FY also would like to thank Dr Duane Carey and Dr Dave Harrison from the University of Leeds for useful discussions on image segmentation. Authors acknowledge financial support from the HEIF Kick Start fund on Software development and commercialisation of cell tracking algorithms.

Appendix A. Supplementary material

All the data for this paper is contained inclusively in this article and Supplementary data associated with this paper can be found in the online version at http://dx.doi.org/10.1016/j.jbiomech.2016.02.008.

References

Blazakis, K.N., Madzvamuse, A., Reyes-Aldasoro, C.C., Styles, V., Venkataraman, C., 2015. Whole cell tracking through the optimal control of geometric evolution laws. J. Comput. Phys. 297, 495–514.

Blowey, J., Elliott, C., 1993. Curvature dependent phase boundary motion and parabolic double obstacle problems. In: Degenerate Diffusions, vols. 51, 52, 55. Springer, New York, pp. 19–60.

Bosgraaf, L., Van Haastert, P.J.M., Bretschneider, T., 2009. Analysis of cell movement by simultaneous quantification of local membrane displacement and fluorescent intensities using Quimp2. Cell Motil. Cytoskelet. 66, 156–165.

Brassel, M., Bretin, E., 2011. A modified phase field approximation for mean curvature flow with conservation of the volume, in: Mathematical Methods in the Applied Sciences, Wiley Online Library, vol. 34. pp. 1157–1180.

Cell Tracking Challenge Datasets, ⟨http://www.codesolorzano.com/celltrackingchallenge/Cell_Tracking_Challenge/Datasets.html⟩, (accessed 11.11.15).

Chan, T.F., Vese, L.A., 2001. Active contours without edges. IEEE Trans. Image Process. 10, 266–277.

Crocker, J.C., Grier, D.G., 1996. Methods of digital video microscopy for colloidal studies. J. Colloid Interface Sci. 179, 298–310.

Croft, W., Elliott, C.M., Ladds, G., Stinner, B., Venkataraman, C., Weston, C., 2014. Parameter identification problems in the modelling of cell motility. J. Math. Biol., 1–38.

Debeir, O., Milojevic, D., Leloup, T., Van Ham, P., Kiss, R., Decaestecker, C., 2005. Mitotic tree construction by computer in vitro cell tracking: a tool for proliferation and motility features extraction, in: EUROCON 2005 The International Conference on Computer as a Tool, vol. 2, pp. 1–10.

Denk, W., Strickler, J.H., Webb, W.W., 1990. Two-photon laser scanning fluorescence microscopy. Science 248, 73–76.

Dey, V., Zhang, Y., Zhong, M., 2010. A review on image segmentation techniques with remote sensing perspective. In: Proceedings of the International Society for Photogrammetry and Remote Sensing Symposium (ISPRS10), Vienna, Austria, XXXVIII, pp. 5–7.
DuChateau, P., Zachmann, D., 1989. Applied Partial Differential Equations. Harper & Row, Publishers Inc.
Friedl, P., Alexander, S., 2011. Cancer invasion and the microenvironment: plasticity and reciprocity. Cell 147, 992–1009.
Friedl, P., Gilmour, D., 2009. Collective cell migration in morphogenesis, regeneration and cancer. Nat. Rev. Mol. Cell Biol. 10, 445–457.
Gal, N., Weihs, D., 2012. Intracellular mechanics and activity of breast cancer cells correlate with metastatic potential. Cell Biochem. Biophys. 63, 199–209.
Gelles, J., Schnapp, B.J., Sheetz, M.P., 1988. Tracking kinesin-driven movements with nanometre-scale precision. Nature 331, 450–453.
Gonzalez, R.C., Woods, R.E., Eddins, S.L., 2004. Digital Image Processing: Using MATLAB. Pearson Prentice Hall.
Grynkiewicz, G., Poenie, M., Tsien, R.Y., 1985. A new generation of Ca 2+ indicators with greatly improved fluorescence properties. J. Biol. Chem. 260 (6), 3440–3450.
Hand, A.J., Sun, T., Barber, D.C., Hose, D.R., MacNeil, S., 2009. Automated tracking of migrating cells in phase-contrast video microscopy sequences using image registration. J. Microsc. 234, 62–69.
Haußer, F., Rasche, S., Voigt, A., 2010. The influence of electric fields on nanostructures-simulation and control. Math. Comput. Simul. 80 (7), 1449–1457.
Haußer, F., Rasche, S., Voigt, A., 2012. Control of nanostructures through electric fields and related free boundary problems. In: Constrained Optimization and Optimal Control for Partial Differential Equations, pp. 561–572.
Horn, B.K.P., Schunck, B.G., 1981. Determining optical flow. Artif. Intell. 17, 185–203.
ibidi GmbH, ibidi GmbH home website, ⟨http://www.ibidi.com⟩, (accessed 11.11.15).
Kass, M., Witkin, A., Terzopoulos, D., 1988. Snakes: active contour models. Int. J. Comput. Vis. 1, 321–331.
Li, K., Miller, E.D., Weiss, L.E., Campbell, P.G., Kanade, T., 2006. Online tracking of migrating and proliferating cells imaged with phase-contrast microscopy. In: Proceedings of the 2006 Conference on Computer Vision and Pattern Recognition Workshop (CVPRW'06).
Li, K., Miller, E.D., Chen, M., Kanade, T., Weiss, L.E., Campbell, P.G., 2008. Cell population tracking and lineage construction with spatiotemporal context. Med. Image Anal. 12, 546–566.
Maska, M., Ulman, V., Svoboda, D., Matula, P., Matula, P., Ederra, C., Urbiola, A., Espana, T., Venkatesan, S., Balak, D.M.W., Karas, P., Bolckova, T., Streitova, M., Carthel, C., Coraluppi, S., Harder, N., Rohr, K., Magnusson, K.E.G., Jalden, J., Blau, H.M., Dzyubachyk, O., Krizek, P., Hagen, G.M., Pastor-Escuredo, D., Jimenez-Carretero, D., Ledesma-Carbayo, M.J., Munoz-Barrutia, A., Meijering, E., Kozubek, M., Oritiz-de-Solorzano, C., 2014. A benchmark for comparison of cell tracking algorithms. Bioimage Inform. 30, 1609–1617.
Meijering, E., Dzyubachyk, O., Smal, I., 2012. Methods for cell and particle tracking, Methods Enzymol. 504, 183–200. In: Proceedings of Imaging and Spectroscopic Analysis of Living Cells.
Miura, K., 2005. Tracking movement in cell biology. Adv. Biochem. Eng./Biotechnol. 95, 267–295.
Mosaliganti, K.R., Gelas, A., Megason, S.G., 2013. An efficient, scalable, and adaptable framework for solving generic systems of level-set PDEs. Front. Neuroinform. 7, 35–40.
Otsu, N., 1979. A threshold selection method from gray level histograms. IEEE Trans. Syst. Man Cybern. 9, 62–66.
Pal, N.R., Pal, S.K., 1993. A review on image segmentation techniques. Pattern Recognit. 26, 1274–1294.
Pepperkok, R., Ellenberg, J., 2006. High-throughput fluorescence microscopy for systems biology. Nat. Rev. Mol. Cell Biol. 7, 690–696.
Rabut, G., Ellenberg, J., 2004. Automatic real-time three-dimensional cell tracking by fluorescence microscopy. J. Microsc. 216, 131–137.
Rektorys, K., 1999. Solving Ordinary and Partial Boundary Value Problems. CRC Press LLC.
Reyes-Aldasoro, C.C., Akerman, S., Tozer, G.M., 2008. Measuring the velocity of fluorescently labelled red blood cells with a keyhole tracking algorithm. J. Microsc. 229, 162–173.
Reyes-Aldasoro, C.C., Griffiths, M.K., Savas, D., Tozer, G.M., 2010. CAIMAN: an online algorithm repository for cancer image analysis. Comput. Methods Progr. Biomed. 103, 97–103.
Sacan, A., Ferhatosmanoqlu, H., Coskun, H., 2008. CellTrack: an open-source software for cell tracking and motility analysis. Bioinformatics 24, 1647–1649.
Sbalzarini, I.F., Koumoutsakos, P., 2005. Feature point tracking and trajectory analysis for video imaging in cell biology. J. Struct. Biol. 151, 182–195.
Schneider, C.A., Rasband, W.S., Eliceiri, K.W., 2012. NIH Image to ImageJ: 25 years of image analysis. Nat. Methods 9, 671–675.
Sezgin, M., Sankur, B., 2004. Survey over image thresholding techniques and quantitative performance evolution. J. Electron. Imaging 13, 146–165.
Tardin, C., Cognet, L., Bats, C., Lounis, B., Choquet, D., 1992. Tracking of cell surface receptors by fluorescence digital imaging microscopy using a charge-coupled device camera. Low-density lipoprotein and influenza virus receptor mobility at 4 degrees C. J. Cell Sci. 101, 415–425.
Topman, G., Sharabani-Yosef, O., Gefen, A., 2011. A method for quick, low-cost automated confluency measurements. Microsc. Microanal. 17, 915–922.
Tröltzsch, F., 2010. Optimal Control of Partial Differential Equations: Theory, Methods and Applications, AMS Bookstore, Berlin, vol. 112.
Weigelin, B., Bakker, G.J., Friedl, P., 2012. Intravital third harmonic generation microscopy of collective melanoma cell invasion. IntraVital 1, 1–12.
Wolf, K., te Lindert, M., Krause, M., Alexander, S., te Riet, J., Willis, A.L., Hoffman, R. M., Figdor, C.G., Weiss, S.J., Friedl, P., 2013. Physical limits of cell migration: control by ECM space and nuclear deformation and tuning by proteolysis and traction force. J. Cell Biol. 201, 1069–1084.
Xiao, M., Zhang, L., Kou, W., Miao, Y., Liu, W., 2012. A background reconstruction algorithm based on intensity extremum classification. Adv. Inf. Sci. Serv. Sci. 4, 337–345.
Xie, X., Mirmehdi, M., 2004. RAGS: region-aided geometric snake. IEEE Trans. Image Process., 640–652.
Yang ,F.W., Venkataraman, C., Styles, V., Madzvamuse, A., 2015. A robust and efficient adaptive multigrid solver for the optimal control of phase field formulations of geometric evolution laws. In preparation.
Zimmer, C., Labruyere, E., Meas-Yedid, V., Guillen, N., Olivo-Marin, J., 2002. Segmentation and tracking of migrating cells in video microscopy with parametric active contours: a tool for cell-based drug testing. IEEE Trans. Med. Imaging 21, 1212–1221.